Inorganic Chemistry

Article

pubs.acs.org/IC

Binuclear Ruthenium Complexes of a Neutral Radical Bridging Ligand. A New "Spin" on Mixed Valency

Stephen D. J. McKinnon,[†] Brian O. Patrick,[‡] A. B. P. Lever,*[,§] and Robin G. Hicks*[,†]

[†]Department of Chemistry, University of Victoria, P.O. Box 3065 STN CSC, Victoria, B.C. V8W 3 V6, Canada

[‡]Crystallography Laboratory, Department of Chemistry, University of British Columbia, Vancouver, B.C. V6T 1Z1, Canada

[§]Department of Chemistry, York University, Toronto, Ontario M3J 1P3, Canada

Supporting Information

ABSTRACT: The electronic structures of $(LX)_2Ru(Vd)Ru(LX)_2$ complexes (Vd = 1,5-diisopropyl-3-(4,6-dimethyl-2-pyrimidinyl)-6-oxoverdazyl radical; LX = acac (acetylacetonate) or hfac (hexafluoroacetylacetonate)) in multiple charge states have been investigated experimentally and computationally. The main focus was to probe the consequences of the interplay between the ruthenium ions and the redox-active verdazyl ligand for possible mixed-valent behavior. Cyclic voltammetry studies reveal one reversible reduction and one reversible oxidation process for both complexes; in addition the acac-based derivative possesses a second reversible oxidation. Analysis of a collection of experimental (X-ray structures, EPR, electronic spectra) and computational (TD-DFT (PCM)) data reveal that the ruthenium ancillary ligands (acac vs hfac) have dramatic consequences for the electronic structures of the complexes in all charge states studied. In the hfac series, the neutral complex is best regarded as a binuclear Ru(II) species bridged by a neutral radical ligand. Reduction to give the anionic complex takes place on the verdazyl ligand, whereas oxidation to the cation (a closed shell species) is shared between Vd and ruthenium. For the acac-based complexes, the neutral species is most accurately represented as a Ru(II)/Ru(III) mixed valent complex containing a bridging verdazyl anion, though some bis(Ru(II))-neutral radical character remains. The monocation complex contains a significant contribution from a "broken symmetry" singlet diradical structure, best represented as a bis-Ru(III) system with an anionic ligand, with significant spin coupling of the two Ru(III) centers via the Vd(−1) ligand (calculated $J = -218$ cm^{-1}). The dication, a spin doublet, consists of two Ru(III) ions linked (and antiferromagnetically coupled) to the neutral radical ligand. Computed net σ- and π-back-donation, spin densities, and orbital populations are provided. Time dependent DFT is used to predict the optical spectra and assign experimental data.

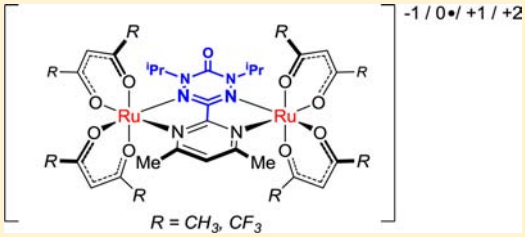

INTRODUCTION

Mixed-valent compounds—species in which an element is present in more than one oxidation state—provide unique opportunities to explore the fundamental interrelationships between delocalization, electron-transfer kinetics, and thermodynamics.[1,2] Such studies are relevant to our understanding of several multimetallic metalloenzymes[3] and to the development of molecular-scale functional materials in which electron transfer/transport plays a key role.[4] By far, the species which have dominated investigations of mixed valency are bimetallic complexes in which two ruthenium ions are connected by a bridging ligand (BL). The mixed valent state is typically accessed by one-electron oxidation of a bis-Ru(II) complex (Scheme 1). Representation of the mixed valent state as having one Ru(II) and one Ru(II) center is a formalism; depending on the nature and magnitude of the interaction between the two metal ions, the mixed-valent state can range from valence-trapped (Robin−Day[5] Class I) to fully delocalized (class III) or somewhere in between (Class II or Class II/Class III border[6]). Understanding the structural and environmental factors which govern the electronic structure of mixed valent complexes is *the* major fundamental goal in this field.

Scheme 1. Formation of Ru(II)/Ru(III) Mixed Valent Complex by Oxidation of a bis-Ru(II) Species

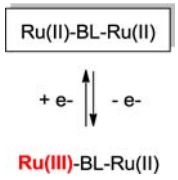

Clearly the BL plays a pivotal role in determining the electronic structure of the mixed valent state. Traditionally the bridge is described as a *mediator* of "electronic coupling" between the two ruthenium ions (two-state model). An interesting subclass of Ru_2 complexes has also been explored in which the BL is explicitly redox active. As genuine three-chromophore systems, such complexes present significantly greater challenges to understand owing to the "additional" redox-active unit. The possibility of the ligand undergoing

Received: March 21, 2013
Published: June 21, 2013

   dx.doi.org/10.1021/ic400704j | *Inorg. Chem.* 2013, 52, 8053−8066

oxidation/reduction events competitive with the ruthenium ions may offer new fundamental phenomena[7] stemming from metal−ligand (in addition to metal−metal) overlap/delocalization and may offer new opportunities for creating or controlling metal−metal interactions for magnetic,[8] optical,[9,10] and conducting[11] properties.

A variety of redox-active BLs have been used to link two ruthenium ions. Conceptually these ligands can be categorized according to their formal charge in their usual "as-synthesized" state, which has direct implications for how their redox-activity is integrated into the more conventional (ruthenium-based) electron transfer chemistry. Scheme 2 depicts electronic structure possibilities for formally dianionic BLs (e.g., *p*-quinonoids,[9,12,13] hydrazides,[14] and π-conjugated hydrocarbons[15]). A conventional (Ru(II)/Ru(III)) state resulting from oxidation of one Ru center is but one possible description of the oxidized form. At the other extreme, ligand-centered oxidation can lead to a ligand radical based complex. Many systems are best described as a blend of these two possibilities, that is, significant metal−ligand delocalization renders assignment of electron transfer locus as metal- or ligand-based inappropriate.

Scheme 2. Electronic Structure Possibilities for Binuclear Ru(II) Complexes Containing Dianionic Redox-Active BLs

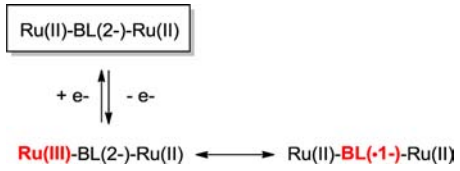

Scheme 3 depicts an alternative scenario, in which a formally neutral but electron-deficient ligand (e.g., azo compounds,[16] nitrogen-rich heterocycles,[17,18] or polynitriles such as TCNE or TCNQ[19]) bridges two Ru(II) centers. Many of these complexes possess near-infrared absorption bands indicative of charge-transfer behavior which can be interpreted as arising from a significant amount of mixed valent character. Oxidation typically leads to "conventional" mixed valent states via oxidation at Ru, whereas reduction is ligand centered and leads to a nonmixed valence state containing the BL as a radical anion.

Scheme 3. Electronic Structure Possibilities for Binuclear Ru(II) Complexes Containing Neutral Redox-Active BLs

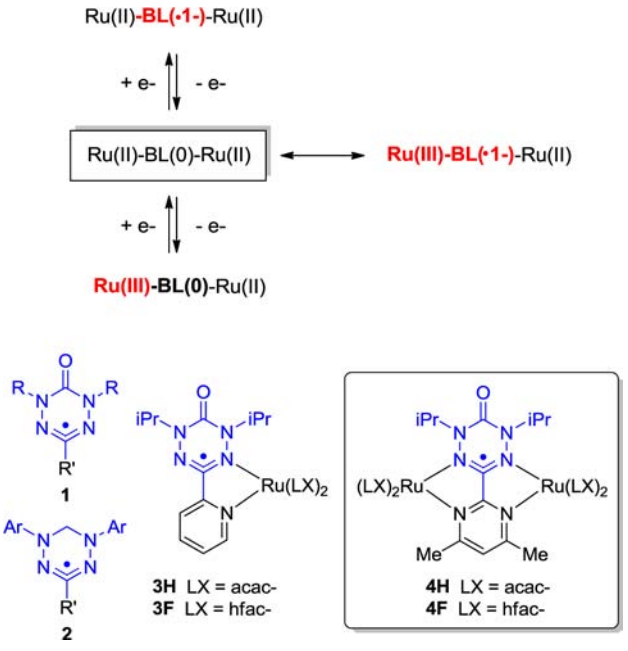

The "ligand radical" states presented in Schemes 2 and 3 are more precisely described as radical *anion* states which are accessed either by oxidation (Scheme 2) or reduction (Scheme 3) of closed-shell ligand species. There are in fact (until this report) *no* examples of binuclear ruthenium complexes which possess a *neutral* radical as the BL (i.e., Ru(II)-BL(•)-Ru(II)). Over the past few years we have been examining the redox properties of verdazyl radicals[20] (**1**,**2**) and their metal complexes.[21] We recently described electronic structure investigations of mononuclear ruthenium bis(diketonate) verdazyl complexes **3H**, **3F**.[22,23] The electronic coupling between ruthenium and the redox-active verdazyl is quite sensitive to the ancillary ligands on Ru and can be quite strong, leading to an exceptional degree of metal−ligand non-innocence.[24] These studies prompted us to consider the consequences of ruthenium-verdazyl coupling and the verdazyl's redox activity in binuclear systems. In this context, we report here the first examples of binuclear ruthenium complexes which are bridged by a neutral radical. Experimental and computational studies are presented for bis-ruthenium complexes **4** in which the BL is a bis-bidentate verdazyl radical.

RESULTS AND DISCUSSION

Synthesis of Neutral Complexes and Model Systems.

The verdazyl ligand 1,5-diisopropyl-3-(4,6-dimethyl-2-pyridinyl)-6-oxoverdazyl (**1a**) was prepared by adaptation of literature procedures for 1,5-diisopropyl-substituted radicals.[25] The binuclear neutral complexes **4H** and **4F** were prepared in high (>80%) yields by the reactions of **1a** with Ru(MeCN)$_2$(LX)$_2$ (LX = acac or hfac for **4H** or **4F** respectively). Both complexes were isolated as crystalline solids. Whereas **4F** is an air-stable material, neutral **4H** is susceptible to air-oxidation to the corresponding cation **4H**$^+$ (see below).

Two model complexes **5H** and **5F** were also prepared in which the bis-bidentate verdazyl **1a** is replaced by the closed-shell BL 4,4′-6,6′-tetramethyl-2,2′-bipyrimidine.[26] These compounds were targeted as (nonradical-containing) models for complexes **4H** and **4F** principally for comparative electrochemical studies (see below). Compound **5H** was initially prepared as its dication (**5H**$^{2+}$.2PF$_6^-$) by reaction of the bipyrimidine ligand with [Ru(MeCN)$_2$(acac)$_2$]PF$_6$. Isolation of the corresponding neutral bis-Ru(II) species **5H** (via reduction of the dication with 2 equiv of cobaltocene) were hampered by its air-sensitivity. The hfac-based species **5F** could be prepared directly from the bipyrimidine and 2 equiv of Ru(MeCN)$_2$(hfac)$_2$.

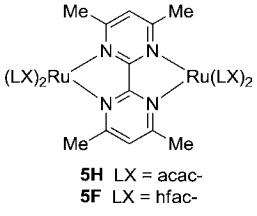

dx.doi.org/10.1021/ic400704j | Inorg. Chem. 2013, 52, 8053−8066

Electrochemical Studies. The redox properties of the two binuclear complexes **4H** and **4F**, verdazyl ligand **1a** and the bipyrimidine analogues **5H** (as its dication) and **5F** were probed using cyclic voltammetry; data are presented in Figure 1

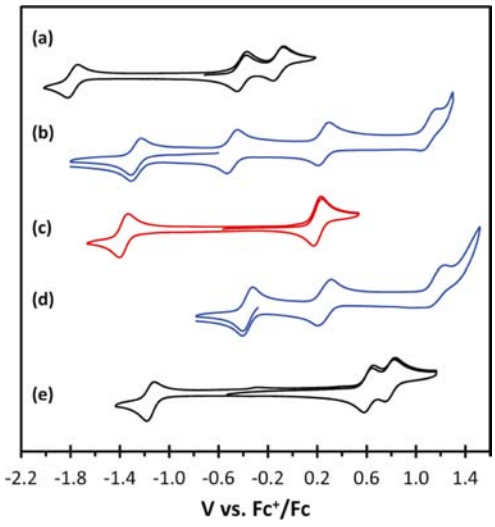

Figure 1. Cyclic voltammograms of (a) $\mathbf{5H}^{2+}$, (b) **4H**, (c) verdazyl ligand **1a**, (d) **4F**, and (e) **5F**. CH_3CN solution, ~1 mM analyte, 0.1 M Bu_4NBF_4 electrolyte, scan rate 100 mV/s.

Table 1. Electrochemical Data (V vs. Fc^+/Fc in CH_3CN)

cpd.	$E^0(0/-1)$	$E^0(+1/0)$	$E^0(+2/+1)$	$E^0(+3/+2)$
1a	−1.35	+0.21		
4H	−1.27	−0.48	+0.25	+1.10[a]
4F	−0.36	+0.26	+1.23[a]	
5H	−1.79	−0.42	−0.13	
5F	−1.15	+0.62	+0.79	

[a]Irreversible process; anodic peak potential reported.

and Table 1. The electrochemical features of the radical ligand are typical,[20] with reversible oxidation and reduction processes evident (Figure 1c). It is convenient to preface discussion of the Ru complexes with the bipyrimidine-bridged species. Both **5H** and **5F** (Figure 1a and 1e respectively) possess two relatively closely spaced oxidation processes which can be assigned to sequential oxidation of each of the two Ru(II) ions, and a reduction process which is bipyrimidine-centered. The oxidation processes for **5F** are about 1 V higher than those for **5H** as expected based on the effects of the hfac vs acac ancillary ligands. The *difference* between the two oxidation steps (ΔE) is 0.29 V for **5H** and 0.17 V for **5F**, again in line with expectations based on the electron withdrawing/donating character of the ancillary ligands.[2] Comproportionation constants[2] for the cationic (mixed valent) states are $10^{4.9}$ and $10^{2.9}$ for **5H** and **5F** respectively; both are modest and consistent with what is most likely to be class II character (though more studies are needed to confirm this).

In the binuclear hfac species **4F** the first reduction and oxidation are much closer to one another compared to the ligand itself; the second oxidation process occurs at a more positive potential and is irreversible. **4H** possesses a triad of redox events which are all reversible and well-separated from one another. The differences between sequential redox events in **4H** correspond to very large comproportionation constants of $10^{13.4}$, $10^{12.4}$, and $10^{14.4}$ for the neutral, cationic, and dicationic forms, respectively. For **4F** the reduction and first oxidation are both reversible and separated by 0.62 V—a much smaller value in comparison to the corresponding ΔE for the free verdazyl (1.56 V), which translates to K_C for the neutral states of **4F** and **1a** of $10^{10.5}$ and $10^{26.4}$, respectively.

Synthesis of Charged Complexes. The monocations $\mathbf{4H}^+$ and $\mathbf{4F}^+$ were prepared by treatment of the corresponding neutral species with $AgPF_6$; because of the significant difference in first oxidation potential of the two neutral complexes the oxidation reactions were performed in MeCN and CH_2Cl_2, respectively; the oxidizing power of Ag^+ is dramatically different in these two solvents.[27] The dication of **4H** can be prepared by reaction of the neutral species with 2 equiv of $AgPF_6$, but the reaction of the (isolated) monocation $\mathbf{4H}^+$ with 1 equiv of $AgPF_6$ turns out to be a superior route in terms of ease of isolation of the product. Chemical reduction of **4F** with cobaltocene gave the anionic complex $\mathbf{4F}^-$ as its cobaltocenium salt; the analogous reaction with **4H** was attempted with the stronger reducing agent decamethylcobaltocene but the $\mathbf{4H}^-$ complex could not be isolated. In our studies on mononuclear Ru(acac) verdazyl complexes similar problems were encountered.[23]

Structural Studies. X-ray structures were obtained for **4H** and its mono- and dication (Figure 3) and **4F**, its monoanion and monocation (Figure 4); pertinent structural data are compiled in Table 2. Binuclear metal complexes in which each metal is a tris(bidentate)-type structural unit can exist as *meso* ($\Delta\Lambda/\Delta\Lambda$) or *rac* ($\Delta\Delta/\Lambda\Lambda$) diastereomers (Figure 2).[28] Crystallographic characterization reveals that the acac-based series (**4H**) remains *rac* as neutral, cation, and dication. In contrast **4F** was characterized as the *meso* form in neutral and cationic state; perhaps most surprising was obtaining the *rac* form of the anion $\mathbf{4F}^-$, which was made from *meso* neutral compound by (presumably outer sphere) reduction. Previous studies on bis-ruthenium complexes have established that the differences in spectroscopic, electrochemical, and so forth properties between stereoisomers of this type are quite small.[13,18,29] Thus, although there are some lingering questions concerning the stereochemical outcomes of the syntheses, the qualitative electronic structures of **4H** and **4F** should be unaffected by which specific isomer is obtained.

Table 2. Selected Experimental X-ray Distances (Å) of Complexes

bond	**4H**[a]	$\mathbf{4H}^+$	$\mathbf{4H}^{2+}$	$\mathbf{4F}^-$	**4F**	$\mathbf{4F}^+$
N1−N2/N3−N4	1.405(3)	1.378(5), 1.378(5)	1.359(3), 1.356(3)	1.425(9), 1.442(9)	1.392(3), 1.382(3)	1.350(9), 1.360(9)
C1−O1	1.218(4)	1.207(5)	1.197(3)	1.220(10)	1.213(3)	1.188(10)
Ru1−N2/Ru2−N4	2.0201(19)	1.964(3), 1.984(3)	2.1140(19), 1.9962(19)	2.043(6), 2.009(7)	1.9961(19), 2.020(2)	1.984(7), 1.980(7)
Ru1−N11/Ru2−N12	2.076(2)	2.060(4), 2.071(3)	2.0806(19), 2.0760(19)	2.084(6), 2.098(6)	2.0882(18), 2.0877(18)	2.074(7), 2.064(7)

[a]In **4H** individual molecules possess rotational symmetry; only one bond metric is given.

dx.doi.org/10.1021/ic400704j | Inorg. Chem. 2013, 52, 8053−8066

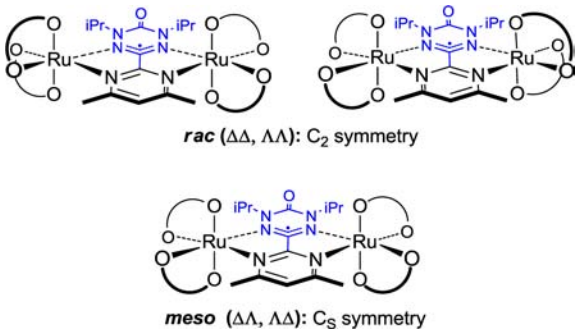

Figure 2. Stereoisomers of **4H** and **4F**.

The tetrazine and pyrimidine rings of the verdazyl ligand in the structure of **4H** (Figure 3a) are very slightly twisted with

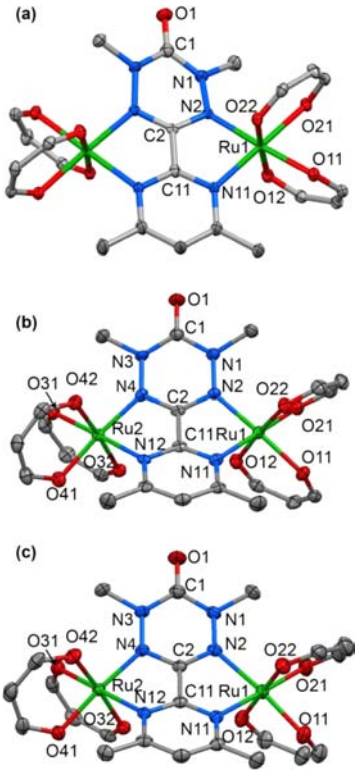

Figure 3. X-ray structures of (a) **4H**, (b) **4H**$^{+}$, and (c) **4H**$^{2+}$. Ellipsoids represented at 50% probability; all hydrogen atoms and the methyl groups of N-isopropyl and β-diketonate moieties removed for clarity.

respect to one another (6.2°). In the cation **4H**$^{+}$ (Figure 3b) the two rings are bent toward one another along the C2−C11 axis, forming an angle of 28.5°. Each Ru ion is displaced from its chelate ring by 0.6 Å on the same face of the Vd ring. As a result each of the two RuO_2 axes (O12−Ru1−O22 and O32−Ru2−O42) tilt toward the other from the ideal perpendicular orientation by an average of 21°. These features are shared by the structure of the dication **4H**$^{2+}$ (Figure 3c); the BL heterocycles are bent toward one another about the C2−C11 axis by 24.4° and the two nominally perpendicular RuO_2 axes are tilted toward each other by an average of 22°.

The structures of **4F** and its corresponding cation and anion are presented in Figure 4; relevant structural metrics are compiled in Table 2. Aside from a change from *rac* to *meso* on going from **4H** to **4F** the gross structural features of the neutral

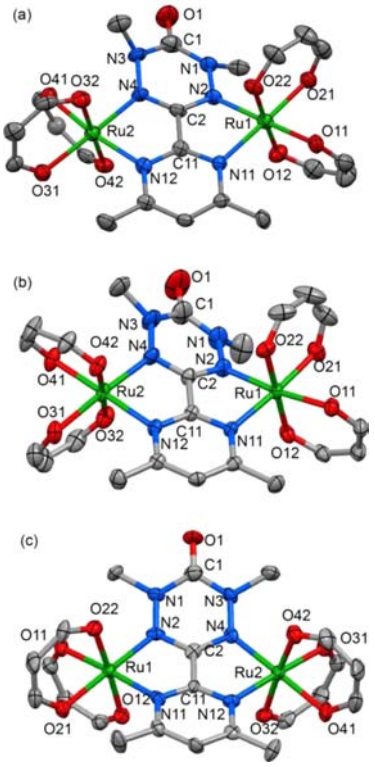

Figure 4. X-ray structures of (a) **4F**$^{-}$, (b) **4F**, and (c) **4F**$^{+}$. Ellipsoids represented at 50% probability; all hydrogen atoms and the methyl groups of N-isopropyl and β-diketonate moieties removed for clarity.

and cationic species are the same, that is, in neutral **4F** the two Ru octahedra are displaced on opposite faces of the Vd ring, whereas in the cation **4F**$^{+}$ they are on the same face leading to a tilting of the two RuO_2 axes. In *rac*-**4F**$^{-}$ the two Ru fragments revert to being on opposite faces. In addition the CN bonds to the isopropyl groups are noncoplanar with the Vd ring; the two methane carbon atoms bound to N1 and N3 are displaced from the tetrazine ring plane by 0.773 and 1.320 Å, respectively. This structural feature was also observed in the anion of the mononuclear Ru-verdazyl compound **3F**.

As we have described for the mononuclear ruthenium-verdazyl complex **3H**,[22,23] the N−N bond lengths in **4H** are somewhat longer (1.405(3) Å) than is the norm for verdazyl complexes of other transition metal ions. Upon oxidation to the mono- and dication, the corresponding N−N bonds become progressively shorter (1.378 and 1.358 respectively). The bond shortening in the cation can be qualitatively understood based on depopulation of the verdazyl radical (N−N antibonding) SOFO (where SOFO, HOFO, and LUFO refer to the SOMO, HOMO, and LUMO of the **F**ragment species respectively), which (assuming changes in charge are accommodated exclusively by the verdazyl) would be empty in the cation. However we have established that in **3H** the Ru(d) to verdazyl (π) backbonding has significant implications for the charge distribution in all charge states. As we discuss below, this also applies in **4H** and in part explains the significant NN bond shortening of the dication structure relative to that of the monocation. Within the **4F** series there is a similar relationship between the overall charge state of the complex and NN bond lengths (see below).

Density Functional Theory Studies. We refer the reader to the general background presented for the mononuclear

dx.doi.org/10.1021/ic400704j | Inorg. Chem. 2013, 52, 8053−8066

verdazyl ruthenium complexes.[23] Here we focus on the impact of the second ruthenium atom and the interaction between the two ruthenium atoms across the verdazyl bridge linkage. In general, we carried out a density functional theory (DFT) geometry optimization looking for the most stable structure. Evidence that the resulting electronic description was viable came from a comparison of the computed and X-ray bond distances (Supporting Information, Table S23), and, likely more meaningful because of packing issues in X-ray data, a good to excellent agreement between the resulting time dependent predicted electronic spectrum and the experimental spectrum (see Electronic Spectra below).

Based on previous experience with these verdazyl species[23] and previous work with noninnocent ligand complexes by Neese, Wieghardt and other groups, *broken symmetry* (BS) ground states involving singlet diradical contributions, are fairly common[30,31] and could be expected here. The broken symmetry formalism was introduced by Noodleman[31] based on unrestricted Hartree−Fock (UHF) wave functions allowing the α- and β-electron to be placed in different orbitals in different parts of the molecule. The broken symmetry orbitals are not spatially orthogonal,[32] and the spin distribution is not adapted to the point group of the molecule, hence the term "broken symmetry". Importantly, the Noodleman broken symmetry approach allows the singlet diradical situation to be approximated by a *single* determinant using UHF wave functions. This method is commonly used to define antiferromagnetic coupling (exchange) constants.[33,34] This formalism, especially in the field of noninnocent ligand chemistry, often provides a UHF description of a singlet state, with an energy more negative than the restricted solution.

The oxidized, neutral, and anionic Vd ligand are represented as Vd(+1), Vd(0), and Vd(−1), respectively, and we use Vd(n) where the oxidation state is undefined. The α-HOFO (SOFO) of Vd(0) is α-#78 which contains one (α) electron.[35] The occupation of this orbital in the various species is listed in Table 3. The presence of approximately two electrons in this orbital will indicate an effective oxidation state of Vd(−1), one electron would be Vd(0), and no electrons or a small fraction of an electron would indicate Vd(+1) as the defining oxidation state.

Table 3. Verdazyl Orbital #78 (Mulliken) and Ruthenium 4d Occupation (NPA) and Derived Dominant Identities

cpd.	Vd #78 occupation	Ru 4d occupation	description of species
4F$^-$	1.84	6.82	[Ru(II)Vd(−1)Ru(II)]$^-$
4F	0.98 (α), 0.27(β)	6.82	Ru(II)Vd(0)Ru(II)
4F$^+$	0.82	6.76	[Ru(III)Vd(0)Ru(II)]$^+$ ⇔ [Ru(II) Vd(+1)Ru(II)]$^+$
4H$^-$	1.91	6.79	[Ru(II)Vd(−1)Ru(II)]$^-$
4H	0.99(α), 0.58(β)	6.79	Ru(III)Vd(−1)Ru(II) ⇔ Ru(II) Vd(0)Ru(II)
4H$^+$ **BS**	0.73(α), 0.73(β)	3.63(α), 3.01(β)[a]	[Ru(III)Vd(−1)Ru(III)]$^+$
4H+ ($^1\Gamma^b$)	1.15	6.72	Ru(III)Vd(−1)Ru(III) ⇔ Ru(III) Vd(0)Ru(II)
4H^{2+}	0.14(α), 0.91(β)	6.58	[Ru(III)Vd(0)Ru(III)]$^{2+}$

[a]For Ru^1; for Ru^2 invert electron labels. [b]Geometry-optimized spin singlet − not the ground state.

The Vd α-HOFO, #78, is a π symmetry orbital spanning the four tetrazine nitrogen atoms and is antibonding with respect to the pair of N−N bonds.[35] Thus, the population of this orbital in the bis-ruthenium complexes (Table 3) influences the N−N bond lengths. Indeed, there is excellent correlation between the orbital occupation numbers and the *computed* N−N bond lengths (Figure 5); complexes with higher occupation numbers

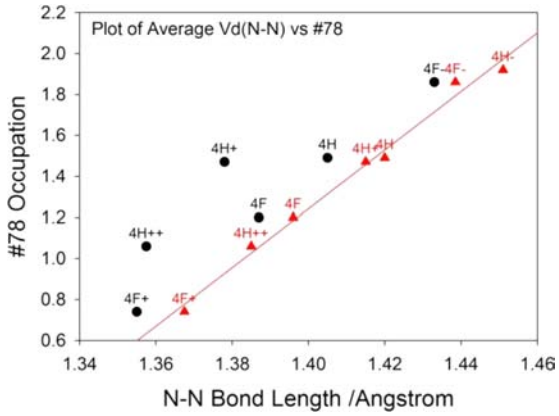

Figure 5. Plot of Vd fragment MO (#78) occupation vs experimental (●) and DFT-calculated (red solid triangles) N−N bond lengths.

have longer bonds. There is also good qualitative agreement between computed orbital occupancy and the experimental N−N bond lengths although clearly there are some discrepancies between experimental and computed bond metrics (particularly in **4H**$^+$ and **4H**$^{2+}$).

Anionic Complexes. **4H**$^-$ and **4F**$^-$ optimized in a straightforward fashion as spin singlet species with close to two electrons in verdazyl fragment MO #78 (Vd(n) (#78 refers to the verdazyl bridge fragment orbital, that is, the SOFO of Vd(0) and the HOFO of Vd(−1). Supporting Information, Figures S1−3,S5 display FMO compositions; more extensive data including MO energies are provided in Supporting Information,Tables S10−S16. With no net spin on ruthenium, these species are easily defined to have the closed shell Ru(II)Vd(−1)Ru(II) core structure. The HOMO of both anionic complexes comprise ruthenium 4d coupled to the HOFO of Vd(−1) (i.e., HOFO #78). The set of six d orbitals ("t_{2g}" in O_h, on each Ru) in **4F**$^-$are relatively unmixed with the ligand orbitals. In **4H**$^-$ five fairly pure d orbitals are evident while the sixth, HOMO-6 (#194) is the in-phase coupled 4d to Vd(HOFO-1) corresponding with the out-of-phase HOMO (#200). No π-back-donation is involved and consequently there is little metal content in the LUMOs. In **4F**$^-$, four orbitals LUMO−LUMO+3 comprise the in- and out-of-phase coupled π *-LUFOs of each hfac unit, while in **4H**$^-$ the lowest pair of virtual orbitals are π* Vd MOs.

Neutral Complexes. **4H** and **4F** were optimized using unrestricted spin. The percent compositions of the frontier orbitals **4F** and **4H** are shown in Supporting Information, Figure S2. There is extensive mixing between metal and acac/hfac orbitals in the frontier filled MOs and little mixing with Vd(n) orbitals except crucially for the Vd(0) HOFO. However there are some low lying virtual Vd π* orbitals so that low lying $ML_{Vd}CT$ and LL′CT transitions can be expected. As noted for the mononuclear systems, the α-HOMO orbitals of these species contain a dominant contribution from the Vd(0) α-HOFO which does not therefore provide for back-donation

dx.doi.org/10.1021/ic400704j | Inorg. Chem. 2013, 52, 8053−8066

and thus the α-LUMOs have little metal content. In the β-manifold, the β-LUMO of Vd is coupled strongly into the β-HOMO-3 of the complex and hence does provide a pathway for π-back-donation. This is reflected in the metal contribution to the β-LUMO of the complexes (Supporting Information, Figure S2). In parallel with the mononuclear species, this is more important in the acac series than in the hfac series since the latter is a much poorer electron donor to the ruthenium center.

In **4F**, the α-occupation of #78 (Vd(n)) (Table 3) is close to unity, while the β-occupation is very small. The spin density (Table 4) reveals predominant spin on Vd(n) as expected and a small spin on the ruthenium atoms due to spin delocalization.[36] These species can then be considered to have the core structure Ru(II)Vd(0)Ru(II) which would be the most simple expectation for the parent uncharged complexes, but with a small contribution from Ru(III)Vd(−1)Ru(II).

Table 4. NBO Spin Densities (DFT, PCM (dichloromethane))

species (spin state)	Ru	acac(-)	Vd(n)
4H ($^2\Gamma$)	0.31(α), 0.31(α)	0.08 (α)	0.30 (α)
4F ($^2\Gamma$)	0.15(α), 0.11 (α)	0.03 (α)	0.72 (α)
4H$^+$ ($^1\Gamma$, BS)	0.62(α), −0.62 (β)	0.11(α), −0.11(β)	0.01 (α)
4H$^+$ ($^3\Gamma^a$)	0.70(α), 0.69 (α)	0.15(α), 0.14(α)	0.3 (α)
4H^{2+} ($^2\Gamma$)	0.66 (α), 0.66 (α)	0.27 (α), 0.27(α)	0.87(β)

[a]Geometry-optimized lowest excited triplet state.

Monocations. A broken symmetry contribution to **4F**$^+$ was obtained, but the additional stabilization energy is extremely small (ca. 56 cm^{-1}) and the $\langle S^2\rangle$ value (0.186) is rather small. Thus the broken symmetry contribution to this electronic structure is not significant and was not further investigated (see discussion below for **4H**$^+$). We therefore adopt the closed shell structure for this species. The cation **4F**$^+$ could be expected to contain either Vd(+1) or Ru(III). Its MO percent composition diagram (Supporting Information, Figure S3) reveals that the LUMO has appreciable ruthenium content. Indeed the LUMO (#296) is composed of 56.7% LUFO of Vd(+1) (#78) which is also mixed 20.0% into HOMO-3 (#292) (antibonding and bonding respectively). This provides a mechanism to transfer 0.4 electrons from ruthenium into #78. We can indeed expect that Vd(+1) should be quite a good π-acceptor. The total contribution to #78 (Table 3) is 0.82e-, somewhat less than unity. Thus we can construe that the **4F**$^+$ species may be regarded as a resonance hybrid of [Ru(II)Vd(+1)Ru(II)]$^+$ and [Ru(III)Vd(0)Ru(II)]$^+$ the latter the more important component, and again with equivalent ruthenium atoms.

In contrast to **4F**$^+$, an unrestricted spin calculation of S = 0 **4H**$^+$ led to a much more stable configuration than the restricted spin calculation (Table 5). This was also marginally more stable (ca. 250 cm^{-1}, Table 5) than the unrestricted, optimized, S = 1 solution. The stabilization energy[33] (Table 5, $E_S - E_{BS}$) derived from uncoupling the spins from the restricted solution to the broken symmetry solution is 3.80 kcal/mol.

Table 5. SCF Energies of 4H$^+$ (Gaussian 09 Calculation, PCM with Dichloromethane)

4H$^+$ state	label	E (Hartrees)	E_{rel} (cm^{-1})
restricted S = 0	E_S	−2520.37140025	1328
unrestricted S = 1[a]	E_T	−2520.37632018	248
unrestricted S = 1[b]	E_{TBS}	−2520.37274584	1033
unrestricted S = 0 BS ($\langle S^2\rangle$ = 0.8657)[c]	E_{BS}	−2520.37745067	0

[a]Geometry optimized S = 1; $\langle S^2\rangle$ = 2.015, after annihilation $\langle S^2\rangle$ = 2.0001. [b]S = 1 single point calculation of the S = 0 BS geometry. [c]After annihilation $\langle S^2\rangle$ = 0.1864.

In the broken symmetry, weak interaction limit, the singlet and triplet diradicals have the same energy and $\langle S^2\rangle$ = 1. A closed shell singlet has $\langle S^2\rangle$ = 0. The percentage of diradical character can be estimated via eq 1:[33]

$$\% = 100[1 - (1 - S^2)^{0.5}] \quad (1)$$

Cation **4H**$^+$ has an $\langle S^2\rangle$ value of 0.87, illustrating substantial diradical character (64%), indeed more than for the mononuclear analogue ($\langle S^2\rangle$ = 0.58[23]). Bachler et al.[33] also discuss the various procedures that have been used to derive the singlet−triplet gap in a singlet diradical species. For reasons discussed therein, in this weak coupling situation, the singlet−triplet gap ($E_S - E_T$) is not simply the energy difference between the relevant singlet (E_{BS}) and triplet (E_T) configurations,. The most general formula is that of Yamaguchi[34,37] (eq 2). Using data in Table 5, eq 2 yields a value of −218 cm^{-1}, compared, for example, with −1656 cm^{-1} for the broken symmetry ground state of a nickel bis-(diiminobenzosemiquinonate) complex.[38]

$$J = -(E_T - E_{BS})/(2 - \langle S^2\rangle) \quad (2)$$

The "corresponding orbital transformation" (COT)[32,33,39] is carried out to deduce just which MOs of the species comprise the "diradical". In this procedure a unitary transformation is carried out on the α- and β-orbital manifolds so that each α-orbital overlaps just one β-orbital. All bar one pair will have an overlap of about 0.99. The pair that has S_{ab} < 0.99 comprises the so-called "magnetic orbitals" which generate the singlet diradical (antiferromagnetic coupling). We derive for **4H**$^+$ one pair with S = 0.41 (compared with S = 0.68 for the mononuclear species[23]).

Inspection of the corresponding pair of orbitals that are antiferromagnetically coupled (Figure 6) is very instructive.

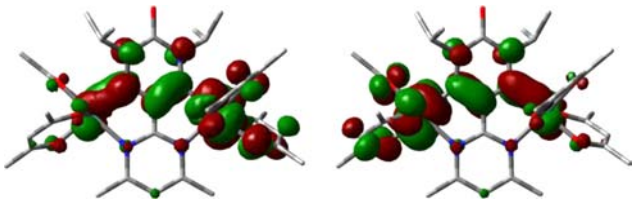

Figure 6. Corresponding (magnetic) orbitals of **4H**$^+$. Nominally these are α- and β- orbitals but the labels are arbitrary. H atoms removed for clarity.

dx.doi.org/10.1021/ic400704j | Inorg. Chem. 2013, 52, 8053−8066

Nominally they have equal energy although the DFT program led to a slight difference in energy (48 cm^{-1}) because of the lack of perfect symmetry of the in-silico molecule. Using the ruthenium labels as above, then in the left orbital, Ru^1 is bonding to Vd, while Ru^2 is antibonding, while the reverse is true for the right-hand orbital. These two orbitals then each contribute an equal amount to the bonding description of the diradical.

Cation $\mathbf{4H}^+$ could nominally be expected to contain Vd(+1) or Ru(III), but its diradical character adds extra complexity. Its percent composition diagram (Figure 7) reveals that both the

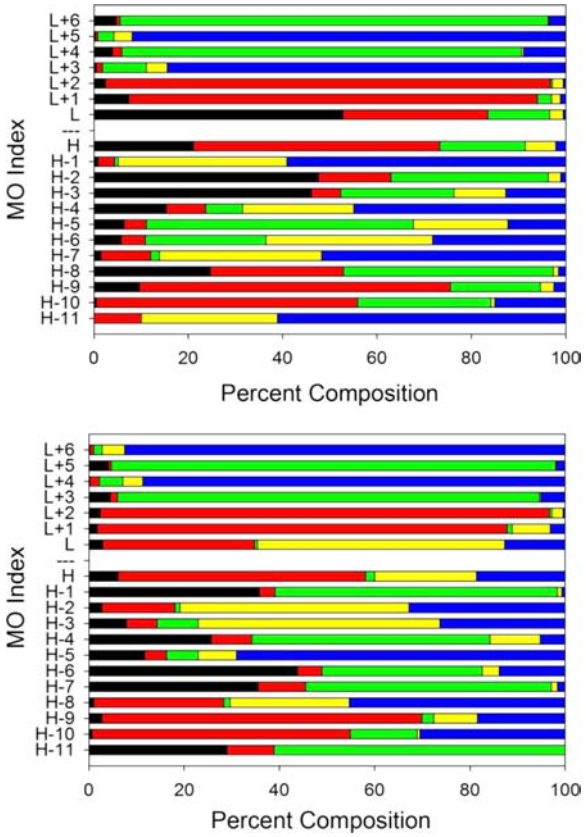

Figure 7. Percent compositions of the frontier orbitals of diradical $\mathbf{4H}^+$. (top, α-; bottom, β- manifolds; HOMO both #199). Code: Ru(III) (Ru^1)(black), Vd (red), acac-1 (green), Ru(III) (Ru^2) (yellow), acac-2 (blue).

α- and β-HOMO levels incorporate coupling between ruthenium 4d and Vd, and analysis shows that it is Vd LUFO (#78) that is mixed into the α- and β-HOMO levels. Within this "broken symmetry" model, each $Ru(acac)_2$ unit behaves fairly independently of the other. We observe that metal containing MOs are mostly labeled black/green or yellow/blue but not both (see Figure 7 and Supporting Information, Figure S4). Further in any given α-MO containing mostly ($Ru^1(acac)_2$) its β-analogue will be mostly ($Ru^2(acac)_2$). For example, the α-LUMO contains a significant contribution from Ru^2, and the β-LUMO contains a significant contribution from Ru^1. Back electron transfer to the Vd(+l) LUFO is therefore important. Indeed Table 3 reveals that the total occupation of #78 is about 1.5 electrons, approaching Vd(−1). Thus contrary to simple expectation, the oxidation of **4H** has led to a species that is best described as Ru(III)Vd(−1)Ru(III). The spin density (Table 4 and Figure 8) shows spin-up and spin-down

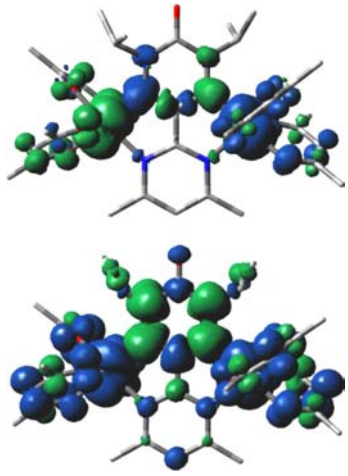

Figure 8. Spin density description of $\mathbf{4H}^+$ (broken symmetry, top) and $\mathbf{4H}^{2+}$ (bottom). H atoms removed for clarity.

Ru(III) species coupled via the Vd(−1) bridge. There is some delocalization of spin onto the adjacent acac units, and some polarization of spin into Vd that crucially, however, has no net spin density (Table 4). However it would be incorrect to assume from the above analysis that the two ruthenium fragments are different. Within this protocol, the real molecule is a 50:50 hybrid of $[Ru^1(III)Vd(-1)Ru^2(III)]^+$ and $[Ru^2(III)Vd(-1)Ru^1(III)]^+$.

In the dication $\mathbf{4H}^{2+}$ (discussed below) the β-manifold LUMO and LUMO+1 each have a significant metal contribution that points to the species having two Ru(III) units. We may question why this is not observed for monocation $\mathbf{4H}^+$. In this case one ruthenium has 3 α-electrons and 2 β-electrons while the other has 3 β-electrons and 2 α-electrons. Thus between the two ruthenium units, one is missing an α-electron (α-LUMO) while the other is missing a β-electron (β-LUMO).

We note that the geometry-optimized closed shell singlet state, lying at about 1300 cm^{-1} above the BS state (Table 5) is also best represented by the electronic structure $[Ru(III)Vd(-1)Ru(III)]^+$, but with a larger contribution from $[Ru(III)Vd(0)Ru(II)]^+$ than the BS state (note the smaller #78 Vd occupancy (Table 3), greater (NBO) positive charge on Vd and less positive charge on Ru (Supporting Information, Table S2)). The geometry optimized triplet state (ca. 250 cm^{-1} above BS ground state) is also best represented by $[Ru(III)Vd(-1)Ru(III)]^+$ (see also Table 4). Thus there are three different electronic descriptions lying very close together in energy.

The dicationic species $\mathbf{4H}^{2+}$ could be expected to be $[Ru(III)Vd(0)Ru(III)]^{+2}$ or $[Ru(III)Vd(+1)Ru(II)]^{+2}$. Indeed direct optimization using unrestricted spin leads to a structure best described as $[Ru(III)Vd(0)Ru(III)]^{+2}$. The significant 4d contributions to the β-LUMO and β-LUMO+1 (Figure 9) allow us to conclude that the complex has two equivalent Ru(III) centers. The corresponding *unoccupied* α-MOs are HOMO (0.82) and HOMO-1 (0.73) (#199,198) (Supporting Information, Figure S5), where the respective overlap coefficients, with the virtual β-MOs (#199,200 respectively), are given in parentheses. A 4d orbital on one ruthenium couples in- and out-of-phase, across the verdazyl bridge, with its partner on the other ruthenium. This gives rise, for example, to α-HOMO, HOMO-1. The deeper α-levels are similarly constructed (Supporting Information, Figure S5 upper) but

dx.doi.org/10.1021/ic400704j | Inorg. Chem. 2013, 52, 8053−8066

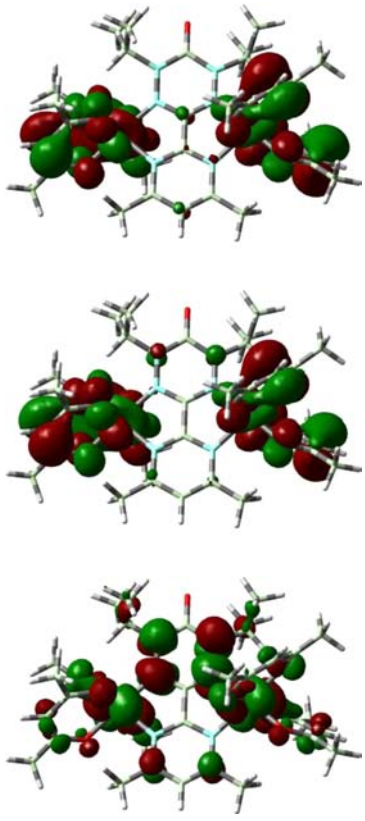

Figure 9. Frontier orbitals of $4H^{++}$. (top) α-HOMO (#199), (middle) α-HOMO-1 (#198), (bottom) β-HOMO (#198).

close analysis shows they are more intermixed than are α-HOMO, HOMO-1.

While it is not quite so obvious, the β-manifold (Supporting Information, Figure S5, lower) is similarly constructed, but rather more mixed. The β-HOMO contains the odd uncoupled β-electron. Its principal α-partner is α-LUMO (overlap 0.73). As shown in Figure 9, this β-electron extends over the verdazyl bridge *and both ruthenium atoms*, but with spin density (−0.81) primarily on the bridge (Table 4). Thus the dicationic species is described to contain a β-electron mostly on the bridge and two α-electrons localized in a pair of in-and-out of phase coupled MOs on each ruthenium atom (spin density +0.66 each). Magnetically, this leads to a net spin of 1/2. The DFT derived expectation value of the $\langle S^2 \rangle$ operator for this species is 1.58. Detailed analysis of this number is outside the scope of this contribution but a simple "zero order" analysis might suppose it reflects a mix of 72% of spin doublet ($\langle S^2 \rangle \geq 0.75$) and 28% of spin quartet ($\langle S^2 \rangle \geq 3.75$).

The energy separation between the α-HOMO and α-HOMO-1 is 234 cm^{-1} indicative of the weak intermetallic coupling across the bridge. For comparison, the next pair, α-HOMO-2,3 are separated by 161 cm^{-1}. The lowest spin quartet (geometry optimized), where the β-spin on the Vd has flipped to α-spin, lies at 617 cm^{-1}. The lowest lying spin doublet excited state (see electronic spectra analysis below) is best described, approximately, by $[Ru(III)Vd(+1)Ru(II)]^{2+}$ and lies at 4,600 cm^{-1}. Thus there are three different electronic descriptions of this species that lie clustered close in energy to each other. Quite possibly some environmental change, for example, choice of solvent, could induce a different ground state, but this was not explored. The relatively poor agreement between the calculated Ru−N(tetrazine) distances and X-ray data (Supporting Information, Table S23) may indeed indicate that the solid state structure differs from that derived from the solution calculation.

A discussion on electron redistribution in this family of compounds, in a comparative sense, can be found in Supporting Information (Table S1 and associated text).

Electronic Spectra. Time dependent DFT[40] was used to predict the optical spectra of these species. The electronic spectra are extraordinarily rich (Figure 10, Table 6) and most experimental "bands" are a summation of many transitions. Since the molecular orbitals are themselves generally a mix of metal, verdazyl, and acac/hfac contributions, the description of a transition as MLCT or LLCT etc. is also rather too facile (see Figure 7, Supporting Information, Figures S1−S3,S5 and Tables S10−S16). It is generally therefore not possible to assign an experimental band in any simple fashion except in cases where only one or two moderately strong transitions make a dominant contribution. Details of the first 80−100 transitions are shown in Supporting Information,Tables S17−S22. Prominent transitions are labeled in Figure 10 and the numbers noted therein, and from the text, are extracted from those tables. We comment briefly here on these dominant contributions.

***4F*$^-$**. Overall agreement between theory and experiment is fairly good with the experimental band envelope being quite well reproduced. Since the HOMO-1 to HOMO-6 are fairly pure d orbitals and LUMO to LUMO+3 are Facac localized (Supporting Information, Figure S1), almost all the lower lying transitions will be primarily $ML_{Fac}CT$. Only transitions from the HOMO which has a large Vd component, will differ, being interligand $L_{Vd}L_{fac}CT$. The low energy band centered around 14,000 cm^{-1} is again evidently composite and likely encompasses predicted transitions (1)−(9) (Supporting Information, Table S17). Reference to Supporting Information, Figure S1 reveals that these are a mix of $ML_{fac}CT$ and $L_{Vd}L_{fac}CT$ and $ML_{Vd}CT$ (from transition (7) terminating on LUMO+4). The visible region band near 22,000 cm^{-1} is clearly highly composite with no simple assignment.

4F. The weak transition (1) near 10000 cm^{-1} is the HOMO to LUMO in the β-manifold and is mainly $4d\pi \rightarrow \pi^*$- verdazyl MLCT with a small d-d transition contribution. The broad experimental band near 13,000 cm^{-1} is highly composite but the strong transition (8) is again $ML_{Vd}CT$ and a small amount of d-d. The band near 25,000 cm^{-1} defies a simple assignment.

***4F*$^+$**. The experimental band envelope is well reproduced by the TD-DFT prediction. Transitions 1 and 2 comprise the near-infrared absorption and are the HOMO and HOMO-1 to LUMO. They are a mix of d-d, $ML_{Vd}CT$, and $L_{ac}L_{Vd}CT$, as indeed is transition (5) which reproduces the experimental band near 11,800 cm^{-1} reasonably well. The next shoulder is fairly well reproduced by transition (7) with a similar mixed assignment as the other transitions but with now some $\pi-\pi^*$ Vd character. The band around 25,000 cm^{-1} is predicted by many overlapping transitions as with the other complexes.

4H. Again the experimental band envelope is well reproduced by the TD-DFT predictions. Transitions (1), (2), and (3) (HOMO, HOMO-1, and HOMO-2 to LUMO, β-manifold, respectively) are assigned to the NIR band and again are a mix of d-d, $ML_{Vd}CT$, and $L_{ac}L_{Vd}CT$. Transition (6) reproduces the next experimental feature and is dominantly α-HOMO to α-LUMO, being a clear $ML_{Vd}CT$ plus some internal

dx.doi.org/10.1021/ic400704j | *Inorg. Chem.* 2013, 52, 8053−8066

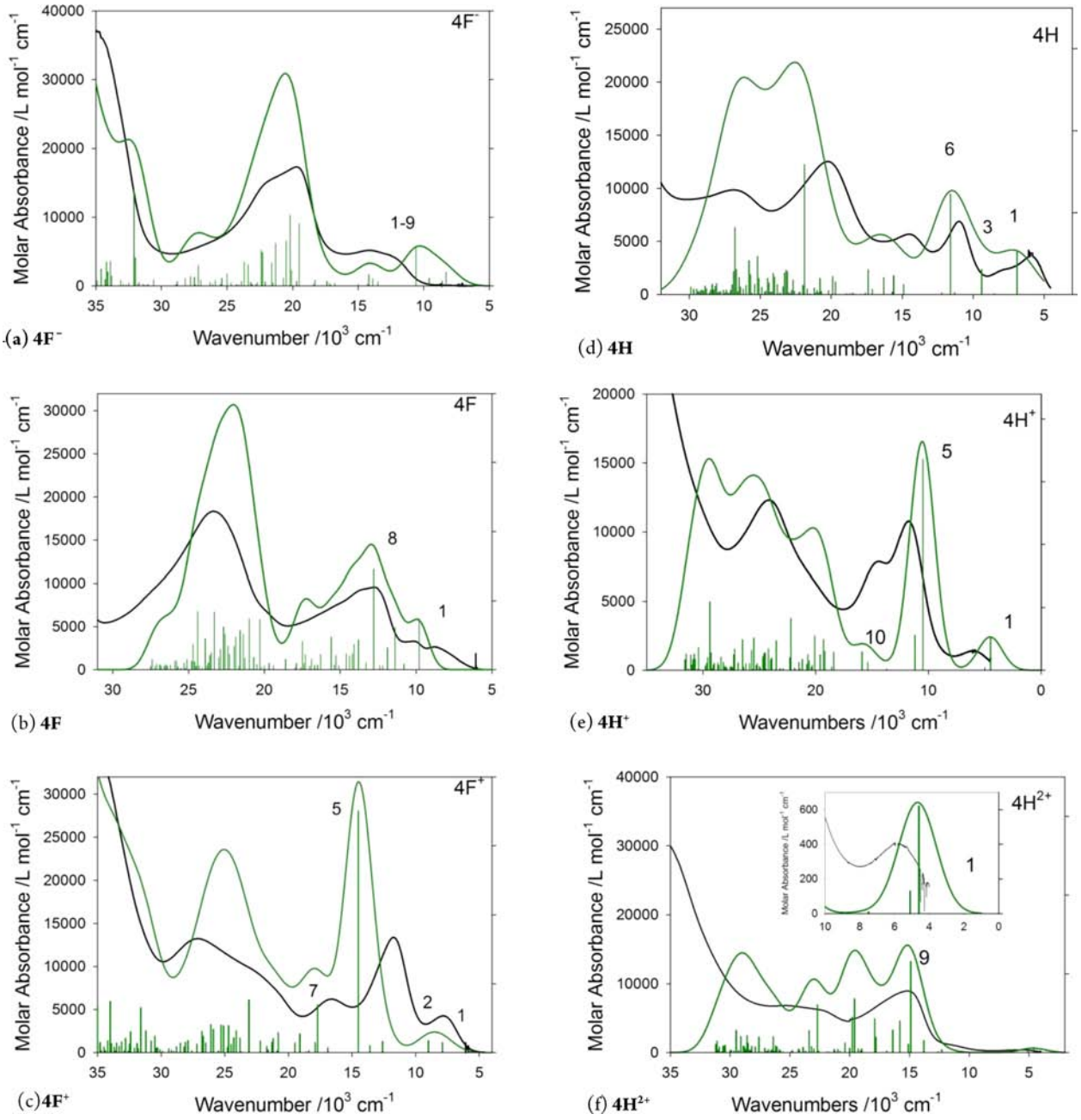

Figure 10. Electronic spectra of (a) $4F^{-}$, (b) **4F**, (c) $4F^{+}$, (d) **4H**, (e) $4H^{+}$, and (f) $4H^{2+}$. Experimental spectra in dichloromethane (black), time dependent DFT calculated spectrum (green) with the location of individual transitions (green bars) with their relative oscillator strengths. Note that the falling off, of the TD-DFT spectra in the UV region, is due to incomplete calculation in the UV because of curtailment of the number of transitions calculated and is not real. Half bandwidths for the TF-DFT calculations are shown in parentheses.

Table 6. Experimental Electronic Spectroscopic Data[a,b]

species	optical spectra (/10^3 cm^{-1} (log ε))
$4F^{-}$	8.3(0.017), *12.50 (3.60)*, 14.12 (3.71), 19.57 (4.24), *21.74 (4.18)*
4F	8.81 (3.42), 10.11 (3.52), 12.77 (3.98), *13.62 (3.97)*, *15.46 (3.85)*, 23.10 (4.26)
$4F^{+}$	7.83 (3.63), 11.68 (4.13), 16.61(3.79), *22.73 (3.95)*, 26.95 (4.12)
4H	5.92 (3.56), *7.84 (3.36)*, 10.94 (3.84), 14.37 (3.75), 20.28 (4.10), 27.03 (3.99)
$4H^{+}$	5.99 (3.15), 11.63 (4.03), 14.43 (3.90), 24.15 (4.09)
$4H^{2+}$	5.88 (2.61), *11.47 (3.06)*, 14.9 (3.95), *22.22 (3.79)*, 25.32 (3.84)

[a]Solvent = dichloromethane; Experimental energy/10^3 cm^{-1}, log molar absorbance in parentheses. [b]Shoulders shown in italics

$\pi-\pi^*$ Vd. Many transitions again lead to a fairly good reproduction of the rest of the experimental spectrum.

***4H*$^+$**. The overall appearance of the spectrum of $4H^+$ is quite similar to that of $4F^+$. The near IR band is well represented by transition (1) being HOMO and HOMO-2 to LUMO in both manifolds. These are a rather complex mix of d-d and $L_{ac}L_{Vd}CT$ (on each end). The strong visible band is assigned as transition (5) with the same description as band (1). The higher energy experimental satellite, near 15,500 cm^{-1}, is assigned to transition (10) which is mostly HOMO to LUMO+1 in both manifolds. This terminates on the bridge and is a fairly well-defined $\pi-\pi^*$ Vd and $ML_{Vd}CT$.

dx.doi.org/10.1021/ic400704j | Inorg. Chem. 2013, 52, 8053−8066

Table 7. Crystallographic Data

	4H	**4H^{+}PF$_6^{-}$**	**4H^{2+}·2PF$_6^{-}$**	**4F**	**4F^{+}PF$_6^{-}$**	CoCp$_2^{+}$**4F^{-}**
empirical formula	$C_{34}H_{49}N_6O_9Ru_2$	$C_{34}H_{49}N_6O_9Ru2PF_6.0.5Et_2O.0.25H_2O$	$C_{34}H_{49}N_6O_9Ru_2.2PF_6$	$C_{34}H_{25}N_6O_9Ru_2F_{24}$	$C_{35}H_{27}N_6O_9F_{30}PCl_2Ru_2$	$C_{44}H_{35}N_6O_9F_{24}Ru_2.CoC_6H_{14}$
formula wt.	887.93	1074.47	1177.87	1319.74	1549.64	1595.02
T (K)	173	173	173	173	173	173
wavelength (Å)	0.71073	0.71073	0.71073	0.71073	0.71073	0.71073
crystal system	monoclinic	monoclinic	monoclinic	triclinic	orthorhombic	monoclinic
space group	$C2/c$ (#15)	$P21/c$ (#14)	$P21/c$ (#14)	$P\bar{1}$ (#2)	$Pna21$ (#33)	$P21/c$ (#14)
a (Å)	23.5778(8)	14.0376(5)	9.4150(2)	12.0677(15)	20.0533(13)	14.2706(9)
b (Å)	23.0939(8)	22.8405(11)	21.9928(5)	12.7539(16)	9.9881(5)	23.2010(17)
c (Å)	8.1395(3)	15.5075(7)	22.5360(6)	16.560(2)	26.4832(17)	17.8901(13)
α (deg)	90	90	90	71.983(5)	90	90
β (deg)	101.639(2)	114.362(2)	97.513(1)	81.323(6)	90	102.025(4)
γ (deg)	90	90	90	89.108(6)	90	90
V (Å^3)	4340.9(3)	4529.4(3)	4626.29(19)	2394.7(5)	5304.4(6)	5793.3(7)
Z	4	4	4	2	4	4
m (cm^{-1})	7.47	7.84	8.26	7.79	8.61	9.35
r_{calc} (g/cm^3)	1.359	1.576	1.691	1.830	1.940	1.829
data collected	11976	74174	50687	51513	31965	32339
unique data	5144	8328	11190	11430	6507	7636
parameters	242	561	603	822	820	805
g.o.f.	1.04	1.09	1.03	1.06	1.08	0.98
R_1	0.050	0.080	0.047	0.040	0.064	0.053
wR_2	0.081	0.089	0.075	0.073	0.095	0.145
CCDC#	804025	804027	804028	804026	804029	804030

dx.doi.org/10.1021/ic400704j | Inorg. Chem. 2013, 52, 8053−8066

$4H^{2+}$. It is gratifying that the very weak feature in the NIR band (Figure 10, Table 6) is well reproduced by theory, with transition (1) which is mostly HOMO → LUMO in the β-manifold. This is primarily a d-d transition with L_{Vd}MCT component (and creates Ru(III)Vd(+1)Ru(II) as noted above). The position of the first intense visible absorption is well reproduced by transition (9) which is composed of HOMO to LUMO+2 in the β-manifold and HOMO-3 to LUMO in the α-manifold. These are a mix of $ML_{Vd}CT$, $L_{ac}L_{Vd}CT$, and $\pi-\pi^*$ Vd. The broad visible range absorption is well predicted by TD-DFT with a large number of moderately strong transitions.

CONCLUSIONS

Complexes **4H** and **4F** represent the first binuclear ruthenium complexes in which the BL is a neutral radical; the redox-activity of the radical bridge demands that these complexes be considered as genuine three-chromophore species. The redox-activity of the radical precludes a straightforward answer to the question of how the presence of an unpaired electron impacts Ru−Ru "communication". Nevertheless, our explorations of the electronic structure of these complexes in several different oxidation states reveal a number of intriguing features. The nature of the ancillary ligands on Ru has a massive impact. This phenomenon was already established in our work on the mononuclear complexes **3H** and **3F**, but in the present systems the second Ru creates a new set of consequences. The electron-withdrawing nature of hfac means that Ru and Vd redox events in **4F** are not very competitive—so Vd redox predominates. The "mixed-valent" (Ru(II)/Ru(III)) state is not accessible here since the Vd ligand is oxidized first, and the subsequent oxidation is not reversible. Reduction of the **4F** is ligand-centered leading to a straightforward description of the anion as Ru(II)Vd(−1)Ru(II). The cationic species obtained upon oxidation is mainly metal centered, with a small contribution from Ru(II)Vd(+1)Ru(II) character.

Replacement of hfac with acac coligands creates a totally different scenario in **4H** because the Ru ions are much more easily oxidized. The extent of Ru-radical electronic coupling is exceptional, as demonstrated by the very large separation in potentials between sequential redox events in **4H**. The electron richness of the $Ru(acac)_2$ fragment means that the neutral species is better described as Ru(III)Vd(−1)Ru(II), that is, a classical mixed valent state. The two cationic species are perhaps the most interesting of all. The monocation, $4H^+$, is an $S = 0$ open shell species containing two Ru(III) centers and a verdazyl anion bridge with no net spin density; presented this way, the diamagnetic Vd(−1) ligand mediates strong antiferromagnetic exchange between the two Ru(III) ions. Thus the nominally diamagnetic Vd ligand in this species plays a noninnocent role in mediating interactions between the two Ru(III) ions. Finally, the dicationic $4H^{2+}$ is best described as a three-spin system in which the verdazyl radical couples antiferromagnetically to a pair of weakly coupled ($S = 1$) Ru(III) ions.

EXPERIMENTAL SECTION

General Considerations. All reactions and manipulations were carried out under an argon atmosphere using standard Schlenk or glovebox techniques unless stated otherwise. Solvents were dried and distilled under argon prior to use. All reagents were purchased from Aldrich and used as received. $Ru(LX)_2(MeCN)_2$ (LX = acac[41] and hfac[42]) and 4,4′,6,6′-tetramethyl-2,2′-bipyrimidine[26] were prepared via literature methods. Verdazyl **1a** was prepared by adaptation of standard procedures (see Supporting Information).[25] EPR spectra were recorded on a Bruker EMX EPR instrument equipped with an X-band microwave bridge. Cyclic voltammetry experiments were performed with a Bioanalytical Systems CV50 voltammetric analyzer. Typical electrochemical cells consisted of a three-electrode setup including a glassy carbon working electrode, platinum counter electrode, and silver wire as quasi-reference electrode. Experiments were run at a scan rate of 100 mV/s. Solutions of analyte (∼1 mM) and electrolyte (0.1 M $Bu_4N^+BF_4^-$) were referenced against an internal standard (∼1 mM Fc). Infrared spectra were recorded as KBr pellets using a Perkin-Elmer Spectrum One instrument. UV−vis spectra were recorded using a Cary 50 Scan instrument. Elemental analyses were carried out by Canadian Microanalytical Services Ltd., Vancouver, BC.

Density functional theory (DFT) calculations employed the Gaussian 09 (Revision C.01) program.[43] The computed *xyz* coordinates for all structures are provided in Supporting Information,Tables S3−S9. Optimized geometries were calculated using the B3LYP exchange-correlation functional[44] with the LANL2DZ basis set[45] on all elements except for ruthenium where the triple-ζ def2-TZVP basis set[46] was used. Tight SCF convergence criteria (10^{-8} a.u.) were used for all calculations. The PCM solvation model[31,47] (using dichloromethane) and were checked for stability and equilibrium using the STABLE = OPT and FREQ Gaussian keywords. Vibrational frequency calculations were performed to ensure that the stationary points were minima. Wave functions were checked for stability. The broken symmetry solution is obtained through use of the Gaussian DFT STABLE = OPT keyword used to seek out BS ground states that are more stable than the closed shell singlet state, or indeed may arise directly from an unrestricted spin calculation of the singlet spin species. Molecular orbital (MO) compositions and the overlap populations between molecular fragments were calculated using the AOMix program[48,49] using the Mulliken scheme.[50] Atomic charges were calculated using the Mulliken[50] and natural population analysis[51] methods as provided in Gaussian 09 (C.01). The analysis of the MO compositions, and the charge decomposition analysis was performed using AOMix-CDA. The PCM model[31,52] was used to model solvation assuming dichloromethane as solvent. Time dependent DFT was used to predict the optical spectra, and the output files were analyzed using the SWIZARD program of Gorelsky.[48]

μ-[1,5-Diisopropyl-3-(4′,6′-dimethylpyrimidin-2′-yl)-6-oxoverdazyl]bis[bis(acetylacetonato)ruthenium], 4H. $Ru(acac)_2(MeCN)_2$ (0.177 g, 0.465 mmol) and **1a** (0.067 g, 0.23 mmol) were combined in benzene (50 mL), and the solution was sparged with argon for 30 min. The mixture was refluxed overnight under an argon atmosphere, during which time the solution turned from orange to dark purple-brown. After cooling to room temperature, the solvent was removed in vacuo. The purple oil was purified by column chromatography (neutral alumina, ethyl acetate) to give **4H** as a maroon solid, yield 175 mg (85%). Recrystallization from hexanes gave crystals suitable for X-ray crystallography (Table 7). FT-IR (KBr), /cm^{-1}: 2963 (w), 2923 (w), 1676 (m), 1566 (s), 1514 (s), 1396 (s), 1265 (m), 1199 (w), 1049 (w), 1021 (w), 627 (w). Anal. Calcd for $C_{34}H_{49}N_6O_9Ru_2$: C, 45.99; H, 5.56; N, 9.46. Found: C, 45.94; H, 5.34; N, 9.24.

μ-[1,5-Diisopropyl-3-(4′,6′-dimethylpyrimidin-2′-yl)-6-oxoverdazyl]bis[bis(hexafluoroacetylacetonato)ruthenium] 4F. $Ru(hfac)_2(MeCN)_2$ (0.903 g, 1.51 mmol) and **1a** (0.201 g, 0.696 mmol) were combined in toluene (50 mL), and the mixture was refluxed for 3 days. The intense green solution was cooled to room temperature, and the solvent was removed in vacuo. The crude product was purified by column chromatography (neutral alumina, hexanes/CH_2Cl_2, 3:1) to give **4F** as a deep green solid, yield 750 mg (81.6%). Recrystallization from hexanes gave crystals suitable for X-ray crystallography. FT-IR (KBr) /cm^{-1}: 1712 (w), 1694 (w), 1583 (m), 1464 (m), 1340 (m), 1262 (s), 1208 (s), 1151 (s), 1098 (m), 1050 (w), 803 (w), 694 (w), 600 (w). Anal. Calcd for $C_{34}H_{25}F_{24}N_6O_9Ru_2$: C, 30.94; H, 1.91; N, 6.37. Found: C, 31.09; H, 1.92; N, 6.34.

μ-[1,5-Diisopropyl-3-(4,6-dimethylpyrimidin-2′-yl)-6-oxoverdazyl]bis[bis(acetylacetonato)ruthenium] hexafluoro-

dx.doi.org/10.1021/ic400704j | Inorg. Chem. 2013, 52, 8053−8066

phosphate $4H^+PF_6^-$. Solid $AgPF_6$ (0.028 g, 0.111 mmol) was added to a solution of **4H** (0.100 g, 0.112 mmol) in CH_3CN (10 mL). The color immediately changed from brown to green. After stirring for 10 min, the mixture was filtered through a pad of Celite to remove Ag(s). The product was purified by chromatography (neutral alumina, CH_2Cl_2) to give a dark oil that crystallized with the addition of diethyl ether, yield 72 mg (60%). FTIR (KBr) /cm^{-1}: 1698 (m), 1556 (s), 1518 (s), 1469 (w), 1430 (w), 1372 (m), 1275 (m), 1202 (w), 1061 (w), 843 (s), 557 (w). Anal. Calcd for $C_{34}H_{49}N_6O_9F_6PRu_2 \cdot 0.5C_4H_{10}O \cdot 0.25H_2O$: C, 40.24; H, 5.11; N, 7.82. Found: C, 39.93;H, 4.97; N, 7.84.

μ-[1,5-Diisopropyl-3-(4,6-dimethylpyrimidin-2′-yl)-6-oxoverdazyl]bis[bis(hexafluoroacetylacetonato)ruthenium] Hexafluorophosphate $4F^+PF_6^-$. Solid $AgPF_6$ (0.019 g, 0.75 mmol) was added to **4F** (0.100 g, 0.0758 mmol) in CH_2Cl_2 (10 mL). The color did not change from green, but a precipitate of Ag(s) formed. After stirring for 10 min, diethyl ether was added, and the solution was filtered to remove the Ag(s) precipitate. The solvent was removed in vacuo, and the product was purified by recrystallization from CH_2Cl_2/hexanes to give a dark microcrystalline solid, yield 72.8 mg (66.1%). FTIR (KBr) /cm^{-1}: 1743 (w), 1710 (w), 1592 (s), 1557 (w), 1455 (w), 1430 (m), 1344 (m), 1261 (w), 1210 (w), 1152 (s), 1101 (w), 1060 (w), 950 (w), 841 (m), 807 (w), 748 (w), 698 (w), 635 (w), 601 (w), 558 (w). Anal. Calcd. for $C_{34}H_{25}N_6O_9F_{30}PRu_2$: C, 27.88; H, 1.72; N, 5.74. Found: C, 27.66; H, 1.72; N, 5.72.

μ-[1,5-Diisopropyl-3-(4,6-dimethylpyrimidin-2′-yl)-6-oxoverdazyl]bis[bis(acetylacetonato)ruthenium] bis(hexafluorophosphate) $4H^{2+}\cdot 2PF_6^-$. To a solution of $4H^+PF_6^-$ (0.072 g, 0.070 mmol) in CH_2Cl_2 (10 mL) was added AgPF6 (0.018 g, 0.071 mmol). The color immediately changed from green to blue. After stirring for 10 min, the mixture was filtered to remove Ag(s). The product was purified by recrystallization from CH_2Cl_2 /Et_2O to give $4H^{2+}\cdot 2PF_6^-$ as a blue microcrystalline solid, yield 58 mg (71%). FTIR (KBr) /cm^{-1}: 2931 (w), 1731 (m), 1614 (w), 1523 (s), 1427 (m), 1367 (m), 1322 (m), 1278 (m), 1067 (w), 1028 (w), 940 (w), 842 (s), 694 (w), 657 (w), 557 (m), 467 (w). Anal. Calcd. for $C_{34}H_{49}N_6O_9F_{12}P_2Ru_2$: C, 34.67; H, 4.19; N, 7.14. Found: C, 34.71; H, 4.20; N, 7.06.

Cobaltocenium μ-[1,5-diisopropyl-3-(4,6-dimethylpyrimidin-2′-yl)-6-oxoverdazyl]bis[bis(hexafluoroacetyl-acetonato)-ruthenium] $CoCp_2^+4F^-$. To a solution of **4F** (0.060 g, 0.045 mmol) in degassed CH_2Cl_2 (10 mL) was added cobaltocene (0.0086 g, 0.045 mmol). The solution changed from green to red-brown. After stirring for 10 min, the solution was evaporated under reduced pressure to 5 mL. Degassed hexanes (10 mL) was transferred by canula and layered on the CH_2Cl_2 solution. Over the course of several hours, dark crystals of $CoCp_2^+4F^-$ formed, yield 46 mg (67%). FTIR (KBr) /cm^{-1}: 3122 (w), 2977 (w), 1656 (m), 1600 (w), 1564 (w), 1537 (m), 1477 (m), 1445 (w), 1419 (w), 1327 (m), 1262 (s), 1196 (s), 1148 (s), 1093 (m), 1012 (w), 942 (w), 863 (w), 819 (w), 790 (w), 744 (w), 691 (m), 599 (w), 457 (w). Anal. Calcd for $C_{44}H_{35}N_6O_9F_{24}CoRu_2$: C, 35.03; H, 2.34; N,5.57. Found: C, 34.93; H, 2.27; N, 5.48.

μ-(4,4′,6,6′-Tetramethyl-2,2′ bipyrimidine)bis[bis(acetylacetonato)ruthenium] bis(hexafluorophosphate) $5H^{2+}\cdot 2PF_6^-$. $[Ru(acac)_2(MeCN)_2]PF_6$ (0.159 g, 0.303 mmol) and 4,4′,6,6′-tetramethyl-2,2′-bipyrimidine (0.028 g, 0.131 mmol) were combined in benzene (25 mL), and the mixture was refluxed overnight, during which time the solution turned from deep blue to purple. After cooling to room temperature, the solvent was removed in vacuo. The purple oil was purified by column chromatography (silica, CH_2Cl_2/CH_3CN, 4:1) to give $4H^{2+}\cdot 2PF_6^-$ as deep purple solid, yield 49 mg (34%). FTIR (KBr) /cm^{-1}: 1611 (w), 1524 (s), 1429 (m), 1365 (m), 1329 (m), 1279 (m), 1030 (w), 939 (w), 840 (s), 694 (w), 656 (w), 641 (w), 557 (m), 471 (w). UV–vis-NIR (CH_2Cl_2), λmax/nm (ε/M^{-1} cm^{-1}): 240(27000), 284(34000), 562(9600). Anal. Calcd. for $C_{32}H_{42}N_4O_8F_{12}P_2Ru_2$: C, 34.85; H, 3.84; N, 5.08. Found: C, 34.96; H, 4.01; N, 5.07.

μ-(4,4′,6,6′-Tetramethyl-2,2′-bipyrimidine)-bis[bis(acetylacetonato)ruthenium] 5H. A solution of $5H^{2+}\cdot 2PF_6^-$ (0.068 g, 0.062 mmol) in CH_2Cl_2 (10 mL) was treated with cobaltocene (0.025 g, 0.13 mmol), and the mixture was stirred for 10 min, during which time the solution turned from purple to orange-brown. The solution was filtered, and the solvent removed in vacuo. The crude product was purified by column chromatography (neutral alumina, ethyl acetate) to give **5H** as a brown solid, yield 31 mg (62%). ^1H NMR showed this product to be a mixture of isomers. ^1H NMR ($CDCl_3$), δ/ppm (a/b, 3.8:1): 6.71a and 6.68b (2H), 5.25b and 5.18a (4H), 2.55a and 2.53b (12H), 2.00b and 1.97a (12H), 1.73b and 1.70a (12H). FTIR (KBr) /cm^{-1}: 3069 (w), 2961 (w), 2920 (w), 1566 (s), 1512 (s), 1401 (s), 1382 (m), 1262 (w), 1218 (w), 1188 (w), 1021 (w), 966 (w), 931 (w), 765 (w), 624 (w). UV–vis–NIR (CH_2Cl_2), λmax/nm (ε, M^{-1} cm^{-1}): 273(39000), 467(20000), 781(7000).

μ-(4,4′,6,6′-Tetramethyl-2,2′-bipyrimidine)bis[bis-(hexafluoroacetylacetonato)ruthenium] 5F. $Ru(hfac)_2(MeCN)_2$ (0.323 g, 0.541 mmol) and 4,4′,6,6′-tetramethyl-2,2′-bipyrimidine (0.0560 g, 0.262 mmol) were combined in toluene (30 mL), and the mixture was refluxed for 3 days. The intense green solution was cooled to room temperature, and the solvent was removed in vacuo, yielding a deep green solid. Chromatography of the solid (neutral alumina, hexanes/ethyl acetate) gave **5F** as a dark green solid, yield 205 mg (62.9%). The product was purified further by recrystallization from hexanes. ^1H NMR ($CDCl_3$), δ /ppm: 7.19 (s, 2H), 6.24 and 6.22 (s,4H), 2.59 (s, 12H). FTIR (KBr) /cm^{-1}: 1577 (m), 1545 (w), 1515 (w), 1472 (m), 1445 (w), 1339 (m), 1263 (s), 1197 (s), 1150 (s), 1097 (m), 1025 (w), 945 (w), 821 (w), 798 (w), 747 (w), 693 (m), 600 (w). UV–vis-NIR (CH_2Cl_2), λmax/nm (ε/ M^{-1} cm^{-1}): 246(24000), 285(38000), 433(22500), 596(9600), 648(11000). Anal. Calcd for $C_{32}H_{18}N_4O_8F_{24}Ru_2$: C, 30.88; H, 1.46; N, 4.50. Found: C, 30.87; H, 1.42; N, 4.49.

■ ASSOCIATED CONTENT

Ⓢ Supporting Information

Complete reference 43, crystallographic details (CIF format), DFT optimized coordinates and energies, comparisons of calculated and experimental bond lengths, TD-DFT predicted UV/vis spectra, and tables of percent composition of frontier orbitals for all pertinent compounds. This material is available free of charge via the Internet at http://pubs.acs.org.

■ AUTHOR INFORMATION

Corresponding Author

*E-mail: rhicks@uvic.ca (R.G.H.), blever@yorku.ca (A.B.P.L.).

Notes

The authors declare no competing financial interest.

■ ACKNOWLEDGMENTS

We thank the Natural Sciences and Engineering Research Council of Canada for support. Computational work was made possible by the facilities of the Shared Hierarchical Academic Research Computing Network, Ontario, Canada (http://www.sharcnet.ca). We also thank Leonard Slep (Universidad de Buenos Aires) for providing the MATLAB software.

■ REFERENCES

(1) (a) Creutz, C. *Prog. Inorg. Chem.* **1983**, *30*, 1. (b) Taube, H. *Angew. Chem., Int. Ed. Engl.* **1984**, *23*, 329. (c) Crutchley, R. J. *Adv. Inorg. Chem.* **1994**, *41*, 273. (d) D'Alessandro, D. M.; Keene, F. R. *Chem. Rev.* **2006**, *106*, 2270. (e) D'Alessandro, D. M.; Keene, F. R. *Chem. Soc. Rev.* **2006**, *35*, 424. (f) Aguirre-Etcheverry, P.; O'Hare, D. *Chem. Rev.* **2010**, *110*, 4839.

(2) Kaim, W.; Lahiri, G. K. *Angew. Chem., Int. Ed.* **2007**, *46*, 1778.

(3) Solomon, E. I.; Xie, X. J.; Dey, A. *Chem. Soc. Rev.* **2008**, *37*, 623.

(4) (a) Ward, M. D. *Chem. Soc. Rev.* **1995**, *24*, 121. (b) Astruc, D. *Acc. Chem. Res.* **1997**, *30*, 383. (c) McCleverty, J. A.; Ward, M. D. *Acc. Chem. Res.* **1998**, *31*, 842.

(5) Robin, M. B.; Day, P. *Adv. Inorg. Chem. Radiochem.* **1967**, *10*, 247.

(6) (a) Demadis, K. D.; Hartshorn, C. M.; Meyer, T. J. *Chem. Rev.* **2001**, *101*, 2655. (b) Brunschwig, B. S.; Creutz, C.; Sutin, N. *Chem. Soc. Rev.* **2002**, *31*, 168.
(7) Miller, J. S.; Min, K. S. *Angew. Chem., Int. Ed.* **2009**, *48*, 262.
(8) (a) Miller, J. S.; Epstein, A. J. *Chem. Commun.* **1998**, 1319. (b) Carbonera, C.; Dei, A.; Letard, J. F.; Sangregorio, C.; Sorace, L. *Angew. Chem., Int. Ed.* **2004**, *43*, 3136. (c) Tao, J.; Maruyama, H.; Sato, O. *J. Am. Chem. Soc.* **2006**, *128*, 1790. (d) Min, K. S.; DiPasquale, A. G.; Golen, J. A.; Rheingold, A. L.; Miller, J. S. *J. Am. Chem. Soc.* **2007**, *129*, 2360.
(9) Barthram, A. M.; Cleary, R. L.; Kowallick, R.; Ward, M. D. *Chem. Commun.* **1998**, 2695.
(10) (a) Garcia-Canadas, J.; Meacham, A. P.; Peter, L. M.; Ward, M. D. *Angew. Chem., Int. Ed.* **2003**, *42*, 3011. (b) Vickers, S. J.; Ward, M. D. *Electrochem. Commun.* **2005**, *7*, 389. (c) Ward, M. D. *J. Solid State Electrochem.* **2005**, *9*, 778. (d) Kaim, W. *Coord. Chem. Rev.* **2011**, *255*, 2503.
(11) Kato, R. *Bull. Chem. Soc. Jpn.* **2000**, *73*, 515.
(12) (a) Ernst, S.; Hanel, P.; Jordanov, J.; Kaim, W.; Kasack, V.; Roth, E. *J. Am. Chem. Soc.* **1989**, *111*, 1733. (b) Dei, A.; Gatteschi, D.; Pardi, L. *Inorg. Chem.* **1990**, *29*, 1442. (c) Aquino, M. A. S.; Lee, F. L.; Gabe, E. J.; Bensimon, C.; Greedan, J. E.; Crutchley, R. J. *J. Am. Chem. Soc.* **1992**, *114*, 5130. (d) Naklicki, M. L.; Crutchley, R. J. *Inorg. Chim. Acta* **1994**, *225*, 123. (e) Naklicki, M. L.; Crutchley, R. J. *J. Am. Chem. Soc.* **1994**, *116*, 6045. (f) Rezvani, A. R.; Evans, C. E. B.; Crutchley, R. J. *Inorg. Chem.* **1995**, *34*, 4600. (g) Ward, M. D. *Inorg. Chem.* **1996**, *35*, 1712. (h) Keyes, T. E.; Forster, R. J.; Jayaweera, P. M.; Coates, C. G.; McGarvey, J. J.; Vos, J. G. *Inorg. Chem.* **1998**, *37*, 5925. (i) Meacham, A. P.; Druce, K. L.; Bell, Z. R.; Ward, M. D.; Keister, J. B.; Lever, A. B. P. *Inorg. Chem.* **2003**, *42*, 7887. (j) De Biani, F. F.; Dei, A.; Sangregorio, C.; Sorace, L. *Dalton Trans.* **2005**, 3868. (k) Kar, S.; Sarkar, B.; Ghumaan, S.; Janardanan, D.; van Slageren, J.; Fiedler, J.; Puranik, V. G.; Sunoj, R. B.; Kaim, W.; Lahiri, G. K. *Chem.—Eur. J.* **2005**, *11*, 4901. (l) Ghumaan, S.; Mukherjee, S.; Kar, S.; Roy, D.; Mobin, S. M.; Sunoj, R. B.; Lahiri, G. K. *Eur. J. Inorg. Chem.* **2006**, 4426. (m) Ghumaan, S.; Sarkar, B.; Maji, S.; Puranik, V. G.; Fiedler, J.; Urbanos, F. A.; Jimenez-Aparicio, R.; Kaim, W.; Lahiri, G. K. *Chem.—Eur. J.* **2008**, *14*, 10816. (n) Grange, C. S.; Meijer, A.; Ward, M. D. *Dalton Trans.* **2010**, *39*, 200. (o) Weisser, F.; Huebner, R.; Schweinfurth, D.; Sarkar, B. *Chem.—Eur. J.* **2011**, *17*, 5727.
(13) (a) Kumbhakar, D.; Sarkar, B.; Maji, S.; Mobin, S. M.; Fiedler, J.; Urbanos, F. A.; Jimenez-Aparicio, R.; Kaim, W.; Lahiri, G. K. *J. Am. Chem. Soc.* **2008**, *130*, 17575. (b) Maji, S.; Sarkar, B.; Mobin, S. M.; Fiedler, J.; Urbanos, F. A.; Jimenez-Aparicio, R.; Kaim, W.; Lahiri, G. K. *Inorg. Chem.* **2008**, *47*, 5204.
(14) (a) Kaim, W.; Kasack, V.; Binder, H.; Roth, E.; Jordanov, J. *Angew. Chem., Int. Ed. Engl.* **1988**, *27*, 1174. (b) Kasack, V.; Kaim, W.; Binder, H.; Jordanov, J.; Roth, E. *Inorg. Chem.* **1995**, *34*, 1924. (c) Knodler, A.; Fiedler, J.; Kaim, W. *Polyhedron* **2004**, *23*, 701.
(15) (a) Maurer, J.; Winter, R. F.; Sarkar, B.; Fiedler, J.; Zalis, S. *Chem. Commun.* **2004**, 1900. (b) Maurer, J.; Winter, R. F.; Sarkar, B.; Zalis, S. *J. Solid State Electrochem.* **2005**, *9*, 738. (c) Klein, A.; Lavastre, O.; Fiedler, J. *Organometallics* **2006**, *25*, 635. (d) Bruce, M. I.; Costuas, K.; Ellis, B. G.; Halet, J. F.; Low, P. J.; Moubaraki, B.; Murray, K. S.; Ouddai, N.; Perkins, G. J.; Skelton, B. W.; White, A. H. *Organometallics* **2007**, *26*, 3735. (e) Maurer, J.; Sarkar, B.; Kaim, W.; Winter, R. F.; Zalis, S. *Chem.—Eur. J.* **2007**, *13*, 10257. (f) Linseis, M.; Winter, R. F.; Sarkar, B.; Kaim, W.; Zalis, S. *Organometallics* **2008**, *27*, 3321. (g) Fox, M. A.; Farmer, J. D.; Roberts, R. L.; Humphrey, M. G.; Low, P. J. *Organometallics* **2009**, *28*, 5266. (h) Khairul, W. M.; Fox, M. A.; Schauer, P. A.; Yufit, D. S.; Albesa-Jove, D.; Howard, J. A. K.; Low, P. J. *Dalton Trans.* **2010**, *39*, 11605. (i) Pevny, F.; Di Piazza, E.; Norel, L.; Drescher, M.; Winter, R. F.; Rigaut, S. *Organometallics* **2010**, *29*, 5912. (j) Costuas, K.; Rigaut, S. *Dalton Trans.* **2011**, *40*, 5643. (k) Fox, M. A.; Le Guennic, B.; Roberts, R. L.; Brue, D. A.; Yufit, D. S.; Howard, J. A. K.; Manca, G.; Halet, J. F.; Hartl, F.; Low, P. J. *J. Am. Chem. Soc.* **2011**, *133*, 18433. (l) Man, W. Y.; Xia, J. L.; Brown, N. J.; Farmer, J. D.; Yufit, D. S.; Howard, J. A. K.; Liu, S. H.; Low, P. J. *Organometallics* **2011**, *30*, 1852. (m) Wang, L.; Yang, W. W.; Zheng, R. H.; Shi, Q.; Zhong, Y. W.; Yao, J. N. *Inorg. Chem.* **2011**, *50*, 7074. (n) Yao, C. J.; Zhong, Y. W.; Yao, J. N. *J. Am. Chem. Soc.* **2011**, *133*, 15697.
(16) (a) Sarkar, B.; Patra, S.; Fiedler, J.; Sunoj, R. B.; Janardanan, D.; Mobin, S. M.; Niemeyer, M.; Lahiri, G. K.; Kaim, W. *Angew. Chem., Int. Ed.* **2005**, *44*, 5655. (b) Hellmann, M.; Frantz, S.; Kaim, W.; Fiedler, J.; Duboc, C. *Inorg. Chim. Acta* **2006**, *359*, 821.
(17) (a) Kohlmann, S.; Kasack, V.; Roth, E.; Kaim, W. *J. Chem. Soc., Faraday Trans. I* **1989**, *85*, 4047. (b) Kaim, W.; Ernst, S.; Kasack, V. *J. Am. Chem. Soc.* **1990**, *112*, 173. (c) Patra, S.; Sarkar, B.; Maji, S.; Fiedler, J.; Urbanos, F. A.; Jimenez-Aparicio, R.; Kaim, W.; Lahiri, G. K. *Chem.—Eur. J.* **2006**, *12*, 489. (d) Maji, S.; Sarkar, B.; Mobin, S. M.; Fiedler, J.; Kaim, W.; Lahiri, G. K. *Dalton Trans.* **2007**, 2411.
(18) Patra, S.; Sarkar, B.; Ghumaan, S.; Fiedler, J.; Kaim, W.; Lahiri, G. K. *Inorg. Chem.* **2004**, *43*, 6108.
(19) (a) Moscherosch, M.; Waldhor, E.; Binder, H.; Kaim, W.; Fiedler, J. *Inorg. Chem.* **1995**, *34*, 4326. (b) Waldhor, E.; Kaim, W.; Lawson, M.; Jordanov, J. *Inorg. Chem.* **1997**, *36*, 3248. (c) Zalis, S.; Sarkar, B.; Duboc, C.; Kaim, W. *Monatsh. Chem.* **2009**, *140*, 765. (d) Zalis, S.; Winter, R. F.; Kaim, W. *Coord. Chem. Rev.* **2010**, *254*, 1383.
(20) Gilroy, J. B.; McKinnon, S. D. J.; Koivisto, B. D.; Hicks, R. G. *Org. Lett.* **2007**, *9*, 4837.
(21) Anderson, K. J.; Gilroy, J. B.; Patrick, B. O.; McDonald, R.; Ferguson, M. J.; Hicks, R. G. *Inorg. Chim. Acta* **2011**, *374*, 480.
(22) McKinnon, S. D. J.; Patrick, B. O.; Lever, A. B. P.; Hicks, R. G. *Chem. Commun.* **2010**, *46*, 773.
(23) McKinnon, S. D. J.; Patrick, B. O.; Lever, A. B. P.; Hicks, R. G. *J. Am. Chem. Soc.* **2011**, *133*, 13587.
(24) (a) Jorgensen, C. K. *Oxidation Numbers and Oxidation States*; Springer Verlag: New York, 1969. (b) Ward, M. D.; McCleverty, J. A. *J. Chem. Soc., Dalton Trans.* **2002**, 275.
(25) (a) Pare, E. C.; Brook, D. J. R.; Brieger, A.; Badik, M.; Schinke, M. *Org. Biomol. Chem.* **2005**, *3*, 4258. (b) Gilroy, J. B.; Koivisto, B. D.; McDonald, R.; Ferguson, M. J.; Hicks, R. G. *J. Mater. Chem.* **2006**, *16*, 2618.
(26) Vlad, G.; Horvath, I. T. *J. Org. Chem.* **2002**, *67*, 6550.
(27) Connelly, N. G.; Geiger, W. E. *Chem. Rev.* **1996**, *96*, 877.
(28) Keene, F. R. *Chem. Soc. Rev.* **1998**, *27*, 185.
(29) (a) Kelso, L. S.; Reitsma, D. A.; Keene, F. R. *Inorg. Chem.* **1996**, *35*, 5144. (b) D'Alessandro, D. M.; Davies, M. S.; Keene, F. R. *Inorg. Chem.* **2006**, *45*, 1656. (c) Sarkar, B.; Patra, S.; Fiedler, J.; Sunoj, R. B.; Janardanan, D.; Lahiri, G. K.; Kaim, W. *J. Am. Chem. Soc.* **2008**, *130*, 3532. (d) Kumbhakar, D.; Sarkar, B.; Das, A.; Das, A. K.; Mobin, S. M.; Fiedler, J.; Kaim, W.; Lahiri, G. K. *Dalton Trans.* **2009**, 9645.
(30) (a) Arion, V.; Wieghardt, K.; Weyhermueller, T.; Bill, E.; Leovac, V.; Rufinska, A. *Inorg. Chem.* **1997**, *36*, 661. (b) Caballol, R.; Castell, O.; Illas, F.; Moreira, P. R.; Malrieu, J. P. *J. Phys. Chem. A* **1997**, *101*, 7860. (c) Futera, Z.; Klenko, J.; Sponer, J. E.; Sponer, J.; Burda, J. V. *J. Comput. Chem.* **2009**, *30*, 1758. (d) Hopmann, K. H.; Conradie, J.; Ghosh, A. *J. Phys. Chem. B* **2009**, *113*, 10540. (e) Lovell, T.; Han, W. G.; Liu, T. Q.; Noodleman, L. *J. Am. Chem. Soc.* **2002**, *124*, 5890. (f) Nair, N. N.; Schreiner, E.; Pollet, R.; Staemmler, V.; Marx, D. *J. Chem. Theor. Comput.* **2008**, *4*, 1174. (g) Prushan, M. J.; Tomezsko, D. M.; Lofland, S.; Zeller, M.; Hunter, A. D. *Inorg. Chim. Acta* **2007**, *360*, 2245. (h) Spikes, G. H.; Sproules, S.; Bill, E.; Weyhermuller, T.; Wieghardt, K. *Inorg. Chem.* **2008**, *47*, 10935.
(31) Noodleman, L.; Lovell, T.; Han, W. G.; Torres, R. A.; Himo, F. *Comprehensive Coordination Chemistry II*; Elsevier: Oxford, U.K., 2004.
(32) Neese, F. *J. Phys. Chem. Solids* **2004**, *65*, 781.
(33) Bachler, V.; Olbrich, G.; Neese, F.; Wieghardt, K. *Inorg. Chem.* **2002**, *41*, 4179.
(34) (a) Yamaguchi, K.; Tsunekawa, T.; Toyoda, Y.; Fueno, T. *Chem. Phys. Lett.* **1988**, *143*, 371. (b) Ovchinnikov, A. A.; Labanowski, J. K. *Phys. Rev. A* **1996**, *53*, 3946. (c) Adamo, C.; Barone, V.; Bencini, A.; Totti, F.; Ciofini, I. *Inorg. Chem.* **1999**, *38*, 1996.
(35) Gilroy, J. B.; McKinnon, S. D. J.; Kennepohl, P.; Zsombor, M. S.; Ferguson, M. J.; Thompson, L. K.; Hicks, R. G. *J. Org. Chem.* **2007**, *72*, 8062.

(36) Ruiz, E.; Cirera, J.; Alvarez, S. *Coord. Chem. Rev.* **2005**, *249*, 2649.
(37) Nishino, M.; Yamanaka, S.; Yoshioka, Y.; Yamaguchi, K. *J. Phys. Chem. A* **1997**, *101*, 705.
(38) Herebian, D.; Wieghardt, K. E.; Neese, F. *J. Am. Chem. Soc.* **2003**, *125*, 10997.
(39) (a) Amos, A. T.; Hall, G. G. *Proc. R. Soc. London, Ser. A* **1961**, *263*, 483. (b) King, H. F.; Stanton, R. E.; Kim, H.; Wyatt, R. E.; Parr, R. G. *J. Chem. Phys.* **1967**, *47*, 1936.
(40) (a) Casida, M. E.; Jamorski, C.; Casida, K. C.; Salahub, D. R. *J. Chem. Phys.* **1998**, *108*, 4439. (b) Stratmann, R. E.; Scuseria, G. E.; Frisch, M. J. *J. Chem. Phys.* **1998**, *109*, 8218. (c) Burke, K.; Werschnik, J.; Gross, E. K. U. *J. Chem. Phys.* **2005**, *123*, 062206.
(41) Kobayashi, T.; Nishina, Y.; Shimizu, K.; Sato, G. P. *Chem. Lett.* **1988**, 1137.
(42) Baird, I. R.; Rettig, S. J.; James, B. R.; Skov, K. A. *Can. J. Chem.* **1999**, *77*, 1821.
(43) Frisch, M. J. et al. *Gaussian 09*, Revision B.1; Gaussian, Inc.: Wallingford, CT, 2009.
(44) Lee, C. T.; Yang, W. T.; Parr, R. G. *Phys. Rev. B* **1988**, *37*, 785.
(45) (a) Dunning, T. H.; Hay, P. J. *Modern Theoretical Chemistry*; Plenum: New York, 1976; Vol. 3; (b) Hay, P. J.; Wadt, W. R. *J. Chem. Phys.* **1985**, *82*, 270. (c) Hay, P. J.; Wadt, W. R. *J. Chem. Phys.* **1985**, *82*, 299.
(46) (a) Feller, D. *J. Comput. Chem.* **1996**, *17*, 1571. (b) Schuchardt, K. L.; Didier, B. T.; Elsethagen, T.; Sun, L. S.; Gurumoorthi, V.; Chase, J.; Li, J.; Windus, T. L. *J. Chem. Inf. Model.* **2007**, *47*, 1045.
(47) Bickelhaupt, F. M. In *Reviews in Computational Chemistry*; Lipkowitz, K. B., Boyd, D. R. E., Eds.; Wiley: New York, 2000; Vol. *15*, p 1.
(48) Gorelsky, S. I. *AOMIX-CDA Program*; 2005; http://www.sg-chem.net/.
(49) Gorelsky, S. I.; Lever, A. B. P. *J. Organomet. Chem.* **2001**, *635*, 187.
(50) (a) Mulliken, R. S. *J. Chem. Phys.* **1955**, *23*, 1841. (b) Mulliken, R. S. *J. Chem. Phys.* **1955**, *23*, 2338. (c) Mulliken, R. S. *J. Chem. Phys.* **1955**, *23*, 2343. (d) Mulliken, R. S. *J. Chem. Phys.* **1955**, *23*, 1833.
(51) Reed, A. E.; Curtiss, L. A.; Weinhold, F. *Chem. Rev.* **1988**, *88*, 899.
(52) Bickelhaupt, F. M.; Baerends, E. J. In *Reviews in Computational Chemistry*; Lipkowitz, K. B., Boyd, D. R. E., Eds.; Wiley: New York, 2000; Vol. *15*.